Delft University of Technology

Study of surface modes on a vibrating electrowetting liquid lens

Strauch, Matthias; Shao, Yifeng; Bociort, Florian; Urbach, Paul

DOI
10.1063/1.4999562
Publication date
2017
Document Version
Final published version
Published in
Applied Physics Letters

Citation (APA)
Strauch, M., Shao, Y., Bociort, F., & Urbach, P. (2017). Study of surface modes on a vibrating electrowetting liquid lens. *Applied Physics Letters*, *111*(17), Article 171106. https://doi.org/10.1063/1.4999562

Important note
To cite this publication, please use the final published version (if applicable).
Please check the document version above.

Copyright
Other than for strictly personal use, it is not permitted to download, forward or distribute the text or part of it, without the consent of the author(s) and/or copyright holder(s), unless the work is under an open content license such as Creative Commons.

Takedown policy
Please contact us and provide details if you believe this document breaches copyrights.
We will remove access to the work immediately and investigate your claim.

This work is downloaded from Delft University of Technology.
For technical reasons the number of authors shown on this cover page is limited to a maximum of 10.

Study of surface modes on a vibrating electrowetting liquid lens

Matthias Strauch,[a] Yifeng Shao, Florian Bociort, and H. Paul Urbach
Delft University of Technology, 2628CH Delft, The Netherlands

(Received 9 August 2017; accepted 14 October 2017; published online 27 October 2017)

The increased usage of liquid lenses motivates us to investigate surface waves on the liquid's surface. During fast focal switching, the surface waves decrease the imaging quality. We propose a model that describes the surface modes appearing on a liquid lens and predicts the resonance frequencies. The effects of those surface modes on a laser beam are simulated using Fresnel propagation, and the model is verified experimentally. © *2017 Author(s). All article content, except where otherwise noted, is licensed under a Creative Commons Attribution (CC BY) license (http://creativecommons.org/licenses/by/4.0/).* https://doi.org/10.1063/1.4999562

Liquid lenses (LLs) are tools to create small tunable optics without any moving parts. Since the first electrowetting lenses were developed,[1–3] many other techniques have been tested to create a focus-tunable lens, i.e., using membranes and acoustic waves.[4–8] While some techniques never left the lab environment, electrowetting and membrane lenses are available commercially.[9,10] The most popular type of liquid lens uses the electrowetting effect to manipulate a liquid-liquid interface with an external voltage. These lenses use two liquids with similar density to avoid any gravity influences. A major drawback next to the energy consumption is that the lens' speed of operation is limited by the liquid's inertia. When switching between two focal positions too fast, surface waves are created, and as a consequence, the image suffers from aberrations.

While liquid lenses can avoid astigmatism by using several electrodes, in particular, spherical aberration is challenging for example in dual beam auto focussing systems,[11] even without switching the focal length. In membrane based LLs, the thickness of the membrane can be varied to minimize aberrations.[12–16] There are promising developments for electrowetting liquid lenses with multiple liquid interfaces,[17] and it has been shown that spherical aberration can be corrected in micro-lenses by controlling the hydrostatic pressure,[18,19] but there has been no technique for a single electrowetting-only macroscopic LL to tackle the spherical aberration yet. The hope to make use of surface waves caused by fast switching to control, introduce, and correct for aberrations motivates us to study their nature in detail.

The vibrating LL surface will be modelled theoretically, and the limitations of the model described. The optical influence of surface vibrations is simulated and compared to the measurements.

Oscillations on liquid droplets have been studied intensively,[20] including a complete solution for the eigenfrequencies of a viscous droplet in another viscous fluid,[21,22] nonlinear oscillations,[23] and constrained liquid droplets.[24] For simplicity, the liquid is assumed to be incompressible and inviscid.[25,26] The waves on the LL surface are modelled as transverse vibrations of a circular membrane, where the surface tension dominates the stiffness. The shape of an undamped vibration $u(r, \varphi, t)$ on a circular membrane satisfies the wave equation, which is given in polar coordinates by[27]

$$\frac{\partial^2 u}{\partial t^2} = c^2\left(\frac{\partial^2 u}{\partial r^2} + \frac{1}{r}\frac{\partial u}{\partial r} + \frac{1}{r^2}\frac{\partial^2 u}{\partial \varphi^2}\right), \tag{1}$$

where r is the radial coordinate, φ is the angular coordinate, t is the time, and c is the speed of waves on the membrane. c is an unknown constant that resembles the speed of waves on a classical membrane but is not identical to the speed of waves in a more thorough model of a liquid. It has to be determined later on to give meaning to the model. Assuming circular symmetry and the shape displacement to be maximal at $t = 0$, the general bound time-harmonic solution is

$$u = A\cos(2\pi f t) J_0\left(\frac{2\pi f}{c} r\right), \tag{2}$$

where J_0 is the Bessel function of first kind and 0th order, f is the frequency, and A is the amplitude. The step from an undamped vibrating membrane to an undamped liquid surface is a change in boundary conditions. While in the case of a drum, the membrane is fixed at the outer boundary $r = R$, the electrowetting equation[28] fixes its first derivative

$$\left.\frac{\partial u(r,t)}{\partial r}\right|_{r=R,t=0} = -\tan\theta, \tag{3}$$

where θ describes the surface deflection angle compared to the resting surface at the radius of the membrane R. By applying the boundary condition, we get for the amplitude

$$A = \frac{c\tan\theta}{2\pi f J_1\left(\frac{2\pi f}{c} R\right)}. \tag{4}$$

The amplitude allows us to make a prediction of the resonance frequencies of the undamped oscillator. By setting the denominator equal to zero, we get the mode frequencies

$$f_n = \frac{c}{2\pi R} j_{1,n}, \tag{5}$$

[a]Electronic mail: m.strauch@tudelft.nl

 © Author(s) 2017.

where $j_{1,n}$ represents the nth root of the Bessel function of first kind and 1st order. Knowing that the Bessel function of first kind forms orthogonal basis functions, when the argument is scaled, any radially symmetric surface shape can be described as a linear combination of these modes. Controlling these surface vibrations may give us the possibility to temporarily design different surface shapes by superposition, as it is done for example in laser pulse shaping.[29] Measuring the mode frequencies experimentally can be used to determine the nature of the surface vibrations and the shape of the surface.[30] It indicates whether the surface modes appear as predicted by the theory. As it is shown in the following paragraph, the lower mode frequencies are at the order of 100 Hz for the used LL.

Since the theory of an undamped vibrating surface can only be an approximation of the experimental situation, we have to point out a few differences to check afterwards whether the simple undamped model can help to understand the behaviour of the real liquid surface. The used liquid lens is an Arctic 39N0 from Varioptic. The lens consists of two liquids with equal densities to eliminate gravity effects. The shape of the liquid container is not cylindrical as assumed by the model but conical in the vicinity of the liquid interface (see Fig. 1). Hence, the size of the membrane slightly changes during vibration. In the static case, the radius of the interface depends on the LL interface curvature and therefore on the applied voltage U. It can be fitted to the data given in the Arctic 39N0 manual

$$R = (3.193 \pm 0.006) \times 10^{-3}\,\mathrm{m} - (1.25 \pm 0.01) \times 10^{-5} U\,\frac{\mathrm{m}}{\mathrm{V}}. \tag{6}$$

Because the mode frequencies depend on the radius [Eq. (5)], they also depend on the applied voltage amplitudes. For small oscillations as investigated in this paper, the introduced frequency shift is $\approx$1.5%, but it can go up to more than 20% for larger fluctuations. As a consequence, the conical shape of the LL limits the applicability of the model to the first 64 modes for the applied small oscillations, where the frequencies start overlapping. In the case of a flat undisturbed surface, the surface radius is $R = (2.65 \pm 0.01) \times 10^{-3}$ m.

The vibration of a real liquid is damped by the viscosity and the friction at the walls. Therefore, the oscillator has to be driven with an external driving voltage to keep the lens oscillating. The dependence of the deflection angle θ (in radians) on the voltage can be fitted to the data given in the Arctic 39N0 manual

$$\theta = -0.949 \pm 0.007 + (2.27 \pm 0.01) \times 10^{-2} U\,\frac{1}{\mathrm{V}}. \tag{7}$$

When the control voltage amplitude is small and oscillates at or close to a resonance, the liquid surface is a standing wave at the resonance frequency. Since the system is damped, a continuous driving force is required to create a steady oscillation. As follows from Eqs. (4) and (7), the amplitude A of the standing wave depends non-linearly on the voltage U. To keep up the validity of the model, it is necessary to remain within the linear regime of the angle behavior. A simulated comparison of the non-linear model and the linearised model is shown in Fig. 2 for a small voltage oscillation, as used in this publication and an extremely large one. While the amplitude deviation due to linearisation is below 1% for the applied small oscillations, it can go up to more than 25% for larger oscillations. The deviation from the cosine behavior introduces additional frequency components which stimulate multiple modes at the same time during the experiments.

For experimental verification, we use the Arctic 39N0 LL model by Varioptic. The optical power is –5 m^{-1} to 15 m^{-1} for applied voltages ranging from 23 V to 70 V. The focal switching speed is limited to 25 Hz (i.e., 20 ms between the two extreme foci). The refractive indices of the two used liquids are $n_1 = 1.3846$ and $n_2 = 1.4921$ at $\lambda = 632.8$ nm. A flat interface was obtained for a voltage of $U = 43.12$ V. The environment temperature is 21 °C. The diameter of the lens aperture is $d = 3.95$ mm.

A collimated HeNe laser beam with a Gaussian beam profile and a FWHM of 8 mm illuminates the LL surface. The intensity distribution of the modified beam is measured using a camera at a distance of 50 cm behind the LL, i.e., in the Fresnel region (see supplementary material for a drawing of the setup). The experiment was carried out using both an SVS-VISTEK eco655MVGE industrial camera and a Photron SA3 high-speed camera. The high-speed camera was used to sample the lens surface within a single oscillation, while the industrial camera is able to sample it over several oscillation cycles. The image acquisition is synchronized to the voltage supply of the liquid lens.

The simplicity of the setup facilitates simulating and predicting the intensity measurements for different parameters. By fitting the simulated to the measured intensity patterns once, the speed of waves can be determined.

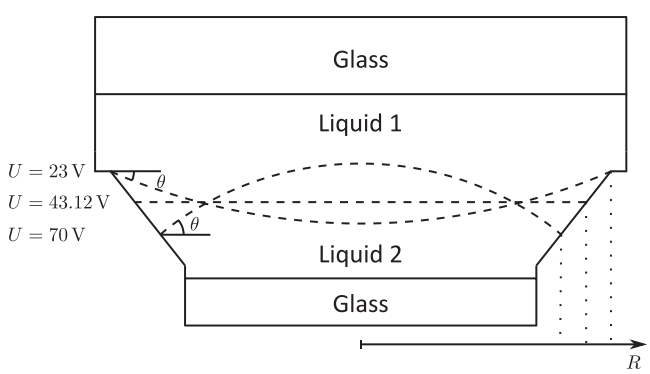

FIG. 1. Schematic profile of the Arctic 39N0 liquid lens. The dashed lines show possible static interface curvatures for different voltages U. θ indicates the deflection angle.

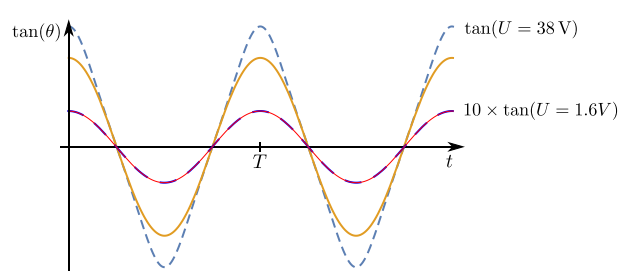

FIG. 2. Comparison of the linear approximation of $\tan(\theta)$ and the exact solution for a small and a large amplitude. The dashed lines show the tangent exactly. The solid lines show the linearisation. To increase readability, the solution for 1.6 V is multiplied by a factor of 10.

The simulation was carried out using both a geometrical optics and a physical optics model. In LightTools, the setup was simulated by means of geometrical optics, but the simulation has not been able to predict the diffraction effects introduced by the lens aperture.

A wave optics model instead delivered promising results. The delay of the incident plane wave is proportional to the optical path length inside the two liquids. The wavefront is propagated to the detector using Fresnel propagation and converted into a relative intensity pattern. The Fresnel approximation is valid for the given aperture diameter and wavelength for distances longer than 1.8 cm behind the liquid lens, which includes our measurement distance sufficiently. For smaller apertures or distances larger than $2d^2/\lambda = 50\,\mathrm{m}$, the simpler Fraunhofer model is sufficiently accurate. The first row of Fig. 3(a) shows the results of the simulated fundamental mode for both extreme surface deflections at $t=0$ and $t=T/2$, where $T=1/f$ is the oscillation period. While the resonance frequencies are predicted by the model, the amplitude can be chosen freely. In the displayed cases, it was chosen to be small, i.e., in the range of 3 μm to 14 μm. The introduced optical path delay is then approximately 0.5–2 wavelengths. The other rows show the higher resonance modes. It can be observed that the amount of dominant rings equals the resonance mode number.

The liquid lens is tuned to a flat surface by applying 43.12 V. A small AC sine signal with an amplitude of 1.6 V is added on top to excite surface modes. The voltage variation is chosen to be small to ensure that the lens surface can be described linearly. The frequency is varied between 10 Hz and 250 Hz. The exposure time of the high-speed camera is 50 μs. The fundamental mode can be identified by comparing the simulated intensity patterns and the experimental data. It occurs at $f_1 = 59\,\mathrm{Hz}$. The next three higher modes can be found in the same way: $f_2 = 108\,\mathrm{Hz}$; $f_3 = 157\,\mathrm{Hz}$; $f_4 = 205\,\mathrm{Hz}$. The appearance of the first four modes is displayed in Fig. 3(b). The left column shows the observed intensity patterns for a maximally deflected surface at $t=0$, and the right column shows the opposite situation for the maximally deflected surface at $t=T/2$. The rows display the measurements of the found resonance frequencies (see supplementary material for a video of the first LL modes). The comparison of the measurements with the simulated intensities shows only minor deviations in the general shape of the light patterns. The measurement of the ground mode at 59 Hz is slightly overexposed and therefore appears to be sharper than the simulation. The small vertical fringe patterns observed throughout the measurements appear due to Fabry-Pérot interference in the camera.

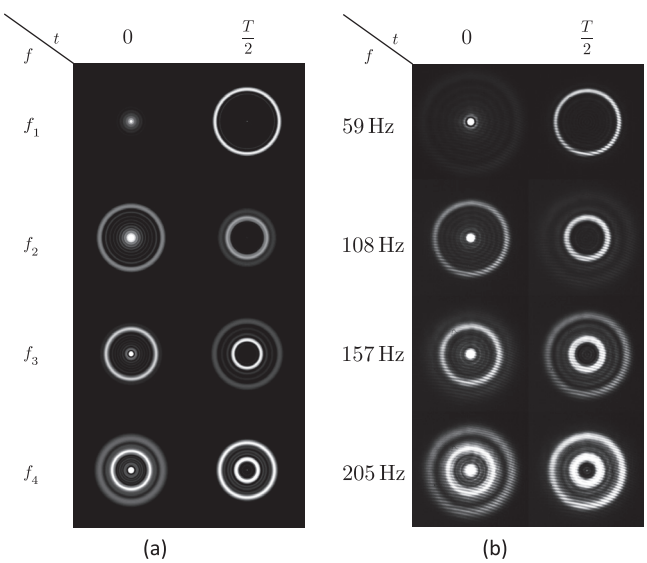

FIG. 3. Comparison of the Fresnel simulation and the measurements of surface waves on a LL. The columns show the intensities produced in both maximally deflected surface situations. (a) Simulation of the intensity pattern for the surface resonances on the LL. The intensity is calculated relative to the input field. (b) High speed camera measurement of the produced intensity patterns. The exposure time is 50 μs.

Using the experimentally determined frequency of the first resonance mode and Eq. (5), the speed of waves on the LL surface can be calculated: $c = 2\pi R f_1/j_{1,1} = (26 \pm 6)$ cm/s. The value is in the expected range for aqueous solutions. This quantity can now be used to predict the behavior of the liquid lens for different voltages and frequencies to create different surface shapes.

The experimentally determined mode frequencies $f_{1,2,3,4}$ are in agreement with Eq. (5). This additionally supports the proposed undamped model. The mode frequencies are much smaller compared to tunable acoustic gradient index of refraction (TAG) lenses[6] (>100 kHz) and allow making the image acquisition more affordable. For higher resonance frequencies though, the resonance frequencies are observed at higher frequencies than predicted by a true Bessel-based surface resonance model. This deviation is probably caused by the larger influence of friction at the walls for higher frequencies, which changes the Neumann boundary condition to a Robin boundary condition.[31]

The influence of damping can be made visible by analysing the frequency response of the system. A way to show the sharpness of the fundamental mode is measuring the intensity on the optical axis at $T=0$ (see Fig. 4). The higher modes are not visible in the graph because the intensity is maximum in the rings surrounding the on-axis peak. The influence of damping is not unexpected since the LL manufacturer artificially increases the damping to optimize the response time and to suppress oscillations.[1]

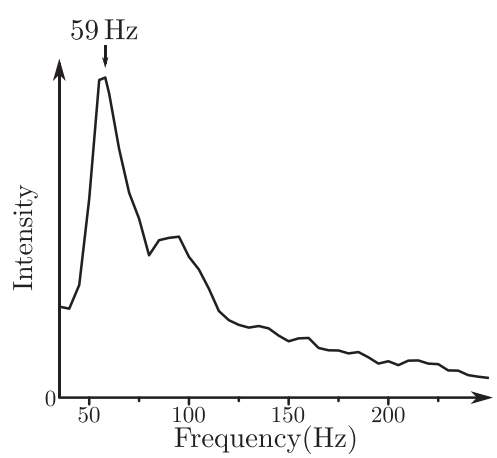

FIG. 4. Intensity on the optical axis versus the modulation frequency at $T=0$. The intensity shows a maximum in the fundamental mode $f_1 = 59\,\mathrm{Hz}$. Higher modes are not visible in the graph since the intensity is split up between the central peak and the surrounding rings.

For high resonance amplitudes, the frequencies also shift and multiple modes are stimulated at the same time. This occurs due to the non-linearity of the model, in both the radius dependency of the resonance frequencies [Eq. (5)] and the tan-dependency of the amplitude [Eq. (4)]. Ultimately, the amplitude of the surface waves is limited by the distance between the glass windows of the LL (comp. Fig. 1).

Surface modes on a liquid lens can be described with a membrane model that is based on the assumption of an inviscid incompressible liquid droplet. The simulated intensity patterns based on a vibrating surface match the experimentally observed behavior. The experimentally dominating low frequency modes can be fully described and predicted with the developed model. High amplitudes and frequencies do not fulfill the approximation since the behavior becomes non-linear and the resonances are highly damped. They therefore only play a minor role in fast focal switching and do not cause relevant aberrations. The obtained knowledge about the surface waves can be used to improve the switching speed of a LL or shape the LL surface such that the phase front can be designed to create a Bessel beam, avoid aberrations (also in 2D imaging), or to create a phase object for digital holography. A publication on the creation of arbitrary aspherical surface shapes based on the proposed model is in preparation.

See supplementary material for an image of the setup and a video of the LL modes.

We acknowledge the use of an educational licence of CODE V and LightTools. This work was funded through the Spectr@phone project (IPD 12017) of the IOP Photonic Devices program of RVO.

[1]B. Berge and J. Peseux, Eur. Phys. J. E **3**, 159 (2000).
[2]T. Krupenkin, S. Yang, and P. Mach, Appl. Phys. Lett. **82**, 316 (2003).
[3]S. Kuiper and B. H. W. Hendriks, Appl. Phys. Lett. **85**, 1128 (2004).
[4]R. Graham, J. Opt. Soc. Am. **30**, 560 (1940).
[5]W. B. Schneider, Physik und Didaktik **2**, 158 (1988).
[6]E. McLeod, A. B. Hopkins, and C. B. Arnold, Opt. Lett. **31**, 3155 (2006).
[7]C. A. López and A. H. Hirsa, Nat. Photonics **2**, 610 (2008).
[8]B. H. W. Hendriks, S. Kuiper, M. A. J. van As, C. A. Renders, and T. W. Tukker, Proc. SPIE **6034**, 603402 (2006).
[9]Invenios France SAS, http://www.varioptic.com/ for Varioptic - liquid lens solutions, auto focus m12 and c-mount lens modules; accessed 26 July 2017.
[10]Optotune, http://www.optotune.com/; accessed 26 July, 2017.
[11]F. Zhang, Y. Yao, X. Qu, T. Zhang, and B. Pei, Opt. Laser Technol. **88**, 198 (2017).
[12]S. Bonora, Y. Jian, P. Zhang, A. Zam, E. N. Pugh, R. J. Zawadzki, and M. V. Sarunic, Opt. Express **23**, 21931 (2015).
[13]M. C. Flores-Bustamante, M. Rosete-Aguilar, and S. Calixto, Proc. SPIE **9699**, 969908 (2016).
[14]H. Huang, K. Wei, Q. Wang, and Y. Zhao, Proc. SPIE **9705**, 970504 (2016).
[15]K. Wei, H. Huang, Q. Wang, and Y. Zhao, Opt. Express **24**, 3929 (2016).
[16]G. Diaz-Gonzalez, A. Santiago-Alvarado, J. Munoz-Lopez, R. Juarez-Salazar, A. S. Cruz-Felix, and N. Jiménez-Barriga, Proc. SPIE **9947**, 99470H (2016).
[17]D. Kopp, T. Brender, and H. Zappe, Appl. Opt. **56**, 3758 (2017).
[18]K. Mishra, C. Murade, B. Carreel, I. Roghair, J. M. Oh, G. Manukyan, D. van den Ende, and F. Mugele, Sci. Rep. **4**, 6378 (2014).
[19]K. Mishra and F. Mugele, Opt. Express **24**, 14672 (2016).
[20]Lord Rayleigh, Proc. R. Soc. London **29**, 71 (1879).
[21]C. A. Miller and L. E. Scriven, J. Fluid Mech. **32**, 417 (1968).
[22]A. Prosperetti, J. Fluid Mech. **100**, 333 (1980).
[23]O. A. Basaran, J. Fluid Mech. **241**, 169 (1992).
[24]J. B. Bostwick and P. H. Steen, Phys. Fluids **21**, 032108 (2009).
[25]L. D. Landau and E. M. Lifshitz, Fluid mechanics, *Course of Theoretical Physics*, Vol. 6, 2nd ed. (Butterworth-Heinemann, London, 2003).
[26]A. Frohn and N. Roth, in *Dynamics of Droplets*, edited by R. J. Adrian, M. Gharib, W. Merzkirch, J. H. Rockwell, and D. Whitelaw (Springer, Berlin, 2000).
[27]P. Hagedorn and A. DasGupta, *Vibrations and Waves in Continous Mechanical Systems* (John Wiley & Sons, Chichester, 2007).
[28]F. Mugele and J.-C. Baret, J. Phys.: Condens. Matter **17**, R705 (2005).
[29]A. M. Weiner, Rev. Sci. Instrum. **71**, 1929 (2000).
[30]M. Kac, Am. Math. Mon. **73**, 1 (1966).
[31]I. Robertson, S. J. Sherwin, and J. M. R. Graham, J. Fluids Struct. **19**, 525 (2004).